

Near-IR images of the torus and micro-spiral structure in NGC 1068 using adaptive optics^{*}

D. Rouan¹, F. Rigaut², D. Alloin³, R. Doyon⁴, O. Lai¹, D. Crampton⁵, E. Gendron¹, and R. Arsenault^{2,1}

¹ Observatoire de Paris, Département Spatial, CNRS URA 264, F-92195 Meudon Cedex, France

² Canada-France-Hawaii Telescope corp., PO Box 1597, Kamuela, Hawaii, 96743, USA

³ Service d'Astrophysique, CNRS URA 2052, CE Saclay, F-91191 Gif-sur-Yvette, France

⁴ Université de Montréal - Département d'Astronomie, C.P. 6128, Succ. A, Montréal, H3C 3J7, Canada

⁵ Dominion Astrophysical Observatory, HIA, National Research Council of Canada, RR5 Victoria, V8X 4M6, Canada

Received 11 December 1997 / Accepted 15 June 1998

Abstract. We present diffraction-limited near-IR images in J, H and K of the nucleus of NGC 1068, obtained with the Adaptive Optics system *Pueo* at CFHT. The achieved resolution ($0''.12$) reveals several components, particularly prominent on the [J–K] image: a) an unresolved, conspicuous core (size < 9 pc); b) an elongated structure at P.A. $\approx 102^\circ$, beginning to show up at radius ≈ 15 pc; c) a S-shaped structure with radial extent ≈ 20 pc, including a bar-like central elongation at P.A. $\approx 15^\circ$ and two short spiral arms. A precise registration of the IR peak was carried out relative to the HST I-band peak. The K unresolved core is found to be close to the location of the putative central engine (radio source S1). Consistent with the Unified Model of AGN, the near-IR core is likely the emission from the hot inner walls of the dust/molecular torus. The extremely red colors of the $0''.2$ diameter core, [J–K]=7.0, [H–K]=3.8, lead to an intrinsic extinction $A_V \geq 2.5$, assuming classical dust grains at 1500 K.

The elongated structure at P.A. $\approx 102^\circ$ may trace the presence of cooler dust within and around the torus. This interpretation is supported by two facts at least: a) the elongated structure is perpendicular to the local radio jet originating at S1; b) its direction follows exactly that of the disk of ionized gas recently found with the VLBA. Regarding the S-shaped feature, the near-IR flux of the bar-like central elongation at P.A. $\approx 4^\circ$, if interpreted in terms of free-free emission from ionized gas, is roughly consistent with the level of 5 GHz emission. However, the radio spectrum behaviour is indicative of synchrotron emission and we rather interpret the $2.2 \mu\text{m}$ emission as originating from warm dust in the shaded part of NLR clouds or in stellar photospheres. The shape itself suggests an extremely compact barred spiral structure, that would be the innermost of a series of nested spiral structures, as predicted by models and simulations. This is supported by the inner stellar distribution – deduced from the J image – which clearly follows an exponen-

tial disk with a 19 pc scale-length, precisely that expected from the rotation of a bar twice this size.

Key words: galaxies: active – galaxies: individual NGC 1068 – galaxies: Seyfert

1. Introduction

Considerable effort has recently been directed towards high spatial resolution imaging of the nucleus of NGC 1068 from UV to radio wavelengths (UV & visible: Macchetto et al. 1994; Capetti et al. 1995, 1997; near-IR: Chelli et al. 1987; Gallais, 1991; Young et al. 1996; Marco et al. 1997; mid-IR: Braatz et al. 1993; Cameron et al. 1993; radio: Wilson & Ulvestad 1987; Planesas et al. 1991; Blietz et al. 1994, Tacconi et al. 1994; Muxlow et al. 1996; Gallimore et al. 1996a,b, 1997; Greenhill & Gwinn 1996). Indeed, as the closest Seyfert 2 nucleus, NGC 1068 deserves such efforts since it is a key object in investigating models of active galactic nuclei (AGN). The popular “Unified” model (e.g., Antonucci 1993) includes a parsec-scale torus of dust and molecular gas around the central engine. Models of the infrared emission from the torus (Krolik & Begelman 1986; Pier & Krolik 1993; Efstathiou & Rowan-Robinson 1994; Granato, Danese & Franceschini 1997) explore torus sizes from 1 to 100 pc. Recently, Gallimore et al. (1997) detected a 1 pc elongated distribution of ionized gas at 8 GHz with the VLBA which they interpreted as the “hot zone” of obscuring material surrounding the AGN. However, direct images showing the torus, or any elongated structure, are still lacking in the near-IR where it is expected to be most conspicuous. To achieve this goal, one requires both high angular resolution ($1'' = 72$ pc at the distance of NGC 1068) and high contrast, the light from the central region being a complex mixture of starlight, synchrotron emission and excited gas emission, all scattered and absorbed by a clumpy dust component.

Near-IR imaging at high angular resolution offers potential advantages in the study of AGN because: *i*) the wavelength range lies between two domains carrying complementary pieces of

Send offprint requests to: D. Rouan (rouan@obspm.fr)

^{*} Based on observations obtained at Canada-France-Hawaii Telescope operated by the National Research Council of Canada, The Centre National de la Recherche Scientifique de France and the University of Hawaii

information – the visible (excited gas in the NLR), and the thermal IR-radio range (cool dust and synchrotron emission from electrons), *ii*) the extinction is reduced, *iii*) diffraction-limited images are now possible thanks to adaptive optics (AO hereafter). Here, we present new results obtained with Pueo, the AO system recently commissioned on the 3.6 m Canada-France-Hawaii Telescope.

2. Observations and results

The CFHT AO system, based on a concept by Roddier et al. (1991), uses a 19 zone bimorph mirror controlled by a curvature wavefront sensor (WFS) to produce diffraction-limited observations (FWHM $\sim 0''.12$) in the near-IR (Rigaut et al., 1994, Lai et al., 1996). The MONICA infrared camera, a facility instrument of the Université de Montréal (Nadeau et al. 1994), was mounted at the output focus of Pueo, itself installed at the Cassegrain focus of CFHT. Special optics in MONICA give a scale on the Nicmos-3 array of $0''.0344$ per pixel.

The observations of NGC 1068, and a nearby blank sky reference position, were obtained on Feb 14, 16 and 18 1997. A dither pattern, with relative offsets of $\sim 0''.8$, was used in order to reduce the effect of bad pixels and to improve the flat-fielding, which was initially derived from dome flats. The UKIRT faint standard stars FS8 and FS7 were used to provide flux and PSF calibrations. The AO system was servoed on the nucleus itself; its rather high brightness and the quality of the seeing (ranging from $0''.38$ in K to $0''.7$ in J) allowed good correction of the turbulence and Strehl ratios of over 60% were obtained at K. The true point spread function (PSF) in each band was recovered using WFS information (Véran et al. 1997). More specifically, it can be shown that departure of a long exposure PSF from a perfect Airy pattern is contributed by : *i*) the non-corrected static aberrations, due for instance to the IR camera optics : these can be measured using an artificial source ; *ii*) the non-perfect compensation by the adaptive mirror of the WF deformations : at low spatial frequencies they are actually measured by the WFS but cannot be completely accommodated by the mirror, while at high spatial frequencies, they are not measured by the WFS, but can be estimated using a Kolmogorov model of the atmosphere, scaled on the actual seeing, itself evaluated from the amplitude of the correction (Véran et al. 1997). Véran (1997) showed that this method for retrieving the real-time PSF is valid, the source being point-like or extended. Similarly, one may wonder if the exactness of the AO correction is maintained, using a slightly extended reference as in the case of NGC 1068¹. Indeed, it has been shown already that the use of an extended source instead of a point-like one to perform the curvature-sensing and AO correction only reduces the efficiency of the WF sensing, but not its accuracy (Rousset, 1994). Moreover, the source extension in the case of NGC 1068 is smaller than the seeing value for all images : in such conditions, even the efficiency loss is small (Eq. 13 in Rousset, 1994). In conclusion, the non point-like shape

of the reference should not introduce systematic errors in the structure of the AO corrected image, nor on the reconstructed PSF. This is illustrated by the comparison between the recovered PSF at K and the image of a nearby star (Fig. 1e, upper left and lower left respectively).

Image processing proceeded as follows: *i*) bad pixel correction; *ii*) sky subtraction, using a median-averaged sky estimate; *iii*) flat-field correction; *iv*) re-centering of the different exposures through cross-correlation techniques; *v*) adjustment of the sky level among the overlapping regions to produce a homogeneous background; *vi*) co-addition of the overlapping regions, rejecting deviant pixels (clipped mean). The resulting images were then deconvolved using the classical Lucy-Richardson algorithm (60 iterations) while following the recipe recently proposed by Magain et al. (1997) to constrain the final PSF.

The un-deconvolved K image is presented in Fig. 1a, on a magnitude (log) scale, chosen because AO provides a high dynamic range (typically $1.3 \cdot 10^4$ at K) and significant details are seen at all flux levels. In Fig. 1e, we show a set of PSF images: the PSFs recovered using the WFS information (Véran et al. 1997) and used in the deconvolution procedure are shown for the 3 bands and, for comparison, the PSF observed in K on a nearby star is also shown. We show in Figs. 1b and d the K and H deconvolved images. Within the $1''$ inner region the following features are visible, especially on the deconvolved K image:

- a) An unresolved core with size less than $0''.12$, i.e. less than 9 pc. The brightest pixel in the core is a factor ≈ 1300 above the background (measured at $6''$ away from the core and showing a mean S/N of 10). This core was known already (Marco et al. 1997), although we can place a more stringent upper limit on its size.
- b) An ESE-WNW elongated structure at PA $\approx 102^\circ$, roughly perpendicular to the axis of the inner ionizing cone (P.A. = 15° , as originally derived by Evans et al., 1991). This structure starts to show up at a radius $0''.20$ with a contrast² of 0.28 in the ESE quadrant and of 0.19 in the WNW quadrant. The mean brightness per pixel of this structure is a factor 340 above the background.
- c) Along the NS direction, a S-shaped feature extends over $0''.3$ on each side of the unresolved core, with a brightness per pixel 200 times the background level. The contrast of the structure at a radius of $0''.2$ is 0.29 to the N and 0.75 to the S. Moreover, within the S-shaped structure, there is an elongation in the direction of the axis of the ionizing cone. We hereafter refer to it as the bar-like structure.

In order to ascertain the reality of the structures we see at faint levels, we have built maps of NGC 1068, of the observed PSF (star) and of the recovered PSF, normalizing the flux at each position (ρ, θ) to the flux averaged along an annulus of the same radius (ρ) . These maps reveal, especially at faint brightness levels (less than 2% of the peak), a few radial structures that are residual aberrations not compensated by AO (mostly due to the

¹ We have measured on the image of NGC 1068, as seen by the WFS (see Sect 2.3), a FWHM of $0''.14$ for the brightest spot on which the AO loop is closed.

² The contrast is defined as $(I_{struct} - I_{avg})/I_{avg}$, i.e. the ratio of the flux excess in the structure at the relevant radius, with respect to the mean inter-structure brightness measured at the same radius.

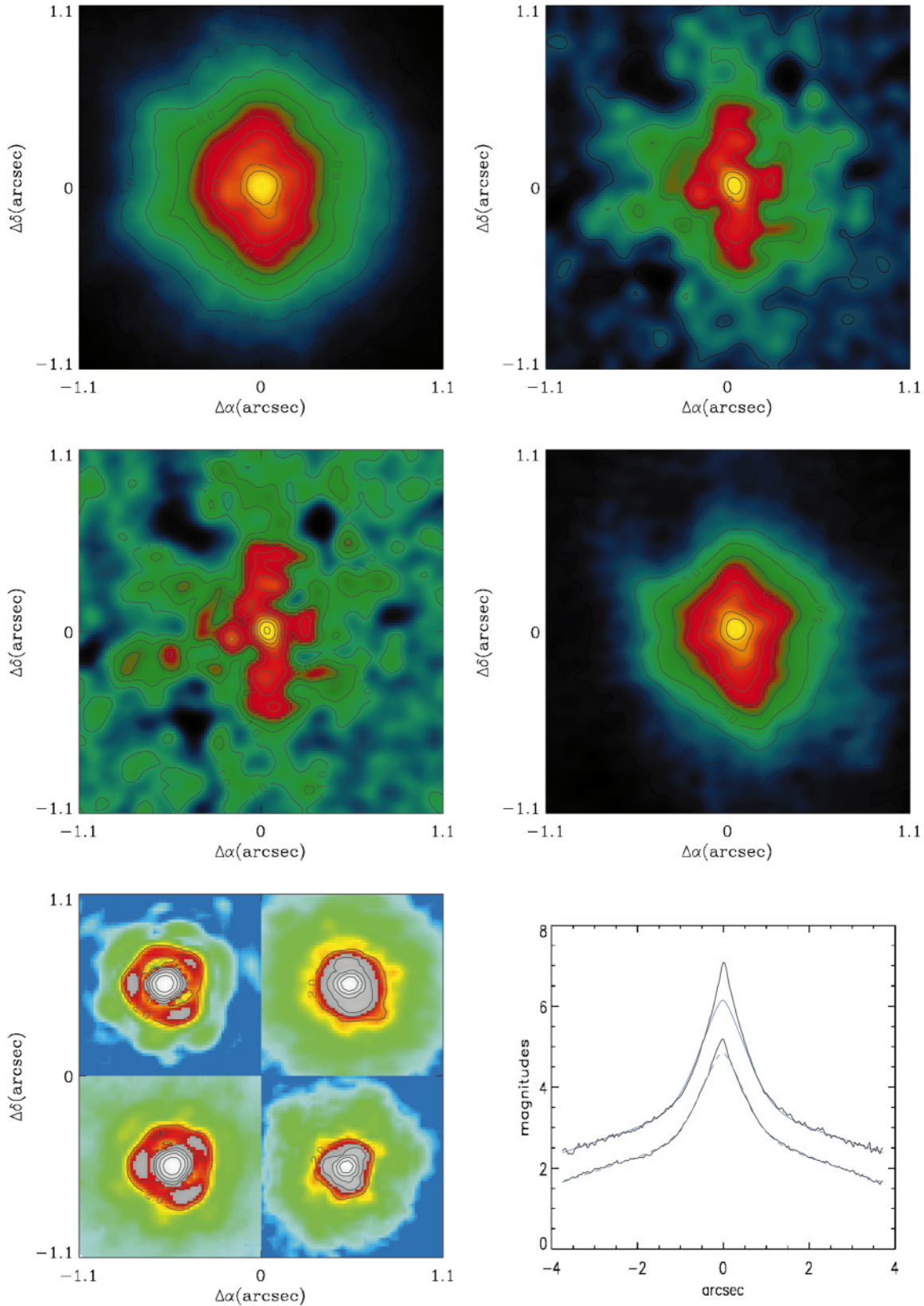


Fig. 1a–f. False color images and isophotes of the $2.2'' \times 2.2''$ area around the nucleus of NGC 1068. For all images, the pixel size is $0''.0344$ and a log (magnitude) scale is used : the step in magnitude between two isophotes is 0.5 for **a,c, d** and **e**, and 1.0 for **b**. From the top, left to right: **a** un-deconvolved K; **b** deconvolved K (see text) ; **c** deconvolved [J–K]; **d** deconvolved H; **e** four panels showing PSF images recovered using the WFS information: upper left – K, upper right – H, lower right – J, lower left – the PSF observed in K on a nearby star; **f** normalized magnitude profiles of a cut at P.A. = 125° in J (lower) and H (upper); a vertical shift has been applied for clarity. For each profile a fit by 2 exponential disks (see text) is also displayed (dashed blue).

camera optics). In particular, a faint feature at P.A. $\approx 50^\circ$ is present on all maps that is clearly such an artifact. However, none of the features in NGC 1068 mentioned above has such a spurious counterpart in the PSF map, and their brightness is well above those of the artifacts.

Owing to the complexity of the central region, we have discarded a simple fit to the stellar distribution in terms of elliptical isophotes. Instead, we assume that the J band emission is a satisfactory representation of the underlying stellar component and we have derived [J–K] and [J–H] color images in order to minimize effects of the stellar component. The [J–K] isophotes (see Fig. 1c) delineate particularly well the three features already mentioned, i.e., the core, the P.A. $\approx 102^\circ$ structure and the S-shaped NS structure. Similar information is also available at $1.65 \mu\text{m}$ in the [J–H] color image (not shown). Neither of the two extended features (b) and (c) is apparent on the J image.

2.1. Photometry of the inner core

Regarding the core observed in J, H and K, integration of the K flux within a $0''.2$ diameter circular diaphragm on the unconvolved image gives $K = 9.3$ mag. PSF fitting with $\text{FWHM} = 0''.12$ gives a result in excellent agreement, confirming that indeed the core is unresolved at $2.2 \mu\text{m}$. In J and H, the contribution of the underlying extended component must first be subtracted. To accomplish this, the J and H profiles at P.A. = 125° , a direction free of the small scale structures discussed previously, were extracted. Beyond $r = 0''.15$, these profiles are quite well fitted by two exponential disks with characteristic radii of $3''.1$ and $0''.26$ (see Fig. 1-f and the discussion in Sect. 3). Once the contribution of the extended component is removed, aperture photometry of the $0''.2$ core gives $J = 16.3$ mag and $H = 13.1$ mag. Assuming that the core centers are coincident in J, H and K, this leads to the extremely red colors $[J-K] = 7.0$ and $[H-K] = 3.8$. For comparison, we find a mean value of $[J-K] = 3.5$ for the regions situated at $r = 0''.2$ either along the P.A. = 102° elongated structure or along the bar-like elongation within the S-shaped feature at P.A. = 4° .

2.2. Large and small scale spiral structures

We compare the inner S-shaped feature with other bar/spiral structures in NGC 1068. From the archived F547M WFPC/HST image in the continuum around 547 nm, one can distinguish (i) an outer barred spiral structure, with the bar at P.A. = 43° , extending over $16''$ in diameter, and (ii) an intermediate barred spiral structure, with the bar at P.A. = 26° , extending over $3''.3$ in diameter. Finally, on the current near-IR images, we find that the inner S-shaped feature shows a bar-like central elongation at P.A. = 4° which extends over a scale of $0''.5$. The existence of interwoven spiral/barred structures in galaxies has been suggested by simulations (Friedli & Martinet, 1993; Heller & Shlosman 1994; Combes 1994a). They are thought to build a fueling channel for the active nucleus in AGN. NGC 1068, in which we detect overlapping spiral structures on three different scales (1.15 kpc, 240 pc, 36 pc) at a P.A. rotating from 43° to 4° inward, appears

to be a good test case for detailed modeling of this effect. This is deferred to a future paper.

2.3. Relative positioning of the near-IR and visible peaks

In order to interpret the new data in the perspective of the AGN modeling, it is necessary to accurately register the near-IR peak with respect to the visible one. One way to achieve this is through simultaneous visible/IR observations, as carried out by Marco et al. (1997), who found the K peak to be offset by $0''.28 \pm 0.05$ S and $0''.08 \pm 0.05$ W from the optical (I band) peak. Here, we have to rely on observations of a nearby star interlaced with the NGC 1068 measurements. This star provides a positional reference both on the WFS and on the near-IR camera. Moreover, because the nearby stellar light source is coincident in the visible and near-IR, any relative offset in the near-IR between the nearby stellar peak and the NGC 1068 peak reflects an intrinsic separation between the visible and the near-IR sources within NGC 1068. However, since the WFS bandpass is rather wide and the central region of NGC 1068 quite complex, the image of NGC 1068 as seen by the WFS has to be generated. Such a composite image was synthesized from archival F502N, F547M, F658N and F791N WFPC2/HST images, kindly made available to us in their fully reduced and precisely aligned form by Z. Tsetanov. These four images were properly scaled, weighted by the WFS response and summed to provide the required image. Because the F547M intensity peak is widely used as the positional reference for the “visible peak” (Lynds et al. 1991) for NGC 1068 research, we have compared the *Pueo* WFS composite image, just obtained above, to the F547M image. We find that the center of gravity of the *Pueo* WFS image is $0''.011$ N and $0''.007$ E of the visible peak. Finally we have derived the offset between the unresolved core on the K image of NGC 1068 and its visible peak to be $0''.180 \pm 0.030$ S and $0''.153 \pm 0.030$ W. This result broadly agrees with that cited above by Marco et al. (1997) and that derived by Thatte et al. (1997) ($0''.216 \pm 0.100$ S and $0''.095 \pm 0.100$ W, as deduced from their Fig. 6, although no indication is given about which image of NGC 1068 was used for the WFS).

3. Discussion and conclusion

Within the remaining uncertainty in the location of the K peak in NGC 1068, we are led to conclude that the unresolved core in K (size less than 9 pc) is coincident with the radio component S1 (Gallimore et al. 1996a), with the $12.4 \mu\text{m}$ source observed by Braatz et al. (1993), and with the center of symmetry of the UV/optical polarization map (Capetti et al. 1995). As a result, we consider that the K unresolved core can be identified with the immediate surroundings of the central engine, most probably with hot dust close to sublimation. Assuming classical dust grains at 1500 K, with associated $[J-K] = 2.76$ and $[H-K] = 1.18$, the extreme red colors of the $0''.2$ diameter core, $[J-K] = 7.0$ $[H-K] = 3.8$ provide an extinction A_V of 25 and 41 mag, respectively (Rieke & Lebofsky 1985). The discrepancy between the two A_V figures obtained remains to be elucidated, and might be related to the nature of the dust grains. We also notice, given

the $0''.12$ resolution of the Pueo data set, that there is some evidence from the profile analysis that the core is resolved in H and J, while this is not the case in K. This result suggests some contribution from scattered light in J and H.

How could we interpret the two extended structures also detected in the K and H bands? The ESE-WNW belt at P.A. = 102° extends over about 20 pc on either side of the core. We argue that it is *very probably the trace of the warm dust within the molecular/dusty torus* invoked in the unified model of AGN since: a) its direction is perpendicular to the axis of the inner ionization cone and to the direction of the radio jet originating from S1; b) its direction follows within 1° that of the small scale (1pc) radio disk recently discovered by Gallimore et al. (1997) with the VLBA and interpreted by these authors as the ionized envelope of the torus; c) the observed K flux ratio of the core to the region at $r = 15$ pc, is the same as the ratio of black body emission at 1500 K and 600 K, respectively; such a set of temperatures and radius is consistent with a simple model of grains heated by a central source ($T_d^5 \propto L_{AGN} r^{-2}$), the hot dust (1500 K) being located at a radius of 1.5 pc and the warm dust (600 K) at a radius of 15 pc.

Concerning the elongated S-shaped feature (± 20 pc on each side of the unresolved core), a first question arises about the emission mechanism at $2.2 \mu\text{m}$. We envisaged that the $2.2 \mu\text{m}$ emission is free-free radiation from ionized gas stripped off the inner edges of the molecular/dusty torus and driven away along the radio axis/inner ionization cone. Under this scenario, the related radio emission at 6cm, proportional to the K emission, would be ≈ 300 mJy, a value in rough agreement with that obtained by Ulvestad et al. (1987). However, this interpretation would be in conflict with the finding by Gallimore et al. (1996a) that the radio emission along the jet (from S1 and up to $\approx 0''.4$ N) has an increasingly steep spectrum, fully consistent with synchrotron emission. We are left with the assumption that the emission at $2.2 \mu\text{m}$ is from stellar photospheres or from warm dust. It is true that the observed [J-K] color, at $r \approx 0''.2$, both along the ESE-WNW belt at P.A. = 102° and along the pseudo-bar within the S-shaped feature, remains very similar, in the range 3.4 to 3.6. As we have seen above, the ESE-WNW belt emission at $2.2 \mu\text{m}$ is consistent with warm dust emission (600K): therefore, we might envisage that the $2.2 \mu\text{m}$ along the pseudo-bar within the S-shaped feature originates from warm dust at the back of NLR clouds shaded from the UV photons in the ionizing cone of the AGN. As a very rough estimate, if we assume a dust temperature of 600K and a black-body emission, then the measured flux of 90 mJy in the $0''.2 \times 0''.3$ area of the pseudo-bar would correspond to a bolometric luminosity of the dust of $1.8 \cdot 10^{10} L_\odot$, i.e. one tenth of the bolometric luminosity of NGC 1068. A lower temperature would lead to much larger luminosities that must be ruled out: for instance $6 \cdot 10^{13} L_\odot$ if $T_{dust} = 300\text{K}$. Starlight is totally unable to produce so large a dust temperature³ and another dust heating mechanism should be invoked: one is direct exposure to X-rays emitted by the cen-

tral engine, another could be shocks, either through direct dust heating within the shock or through secondary heating by UV photons from the shocked gas. The central pseudo-bar may correspond to dust in direct view of the AGN, but then the S-shape would not be explained in this scheme. Shocks at different locations may overcome this difficulty; in terms of energy balance, since models of fast, radiative shocks are indeed able to account for the total number of ionizing photons produced in a Seyfert nucleus (e.g. Dopita & Sutherland, 1995), we can assume that a significant fraction of this UV flux can efficiently heat the dust. On the basis of this sole data set, it is difficult to go beyond this stage in the interpretation of the origin of the $2.2 \mu\text{m}$ photons.

Else, the S-shape is intriguing and might tell us about the origin of the $2.2 \mu\text{m}$ emission. As in the case of NGC 2110 (Mulchaey et al., 1994), we might contemplate an interpretation involving the ejection of optical-emitting gas and radio-emitting gas along the same axis although with different velocities. But then, the emission mechanism at $2.2 \mu\text{m}$ would be dominated by free-free emission which seems to be implausible. We have considered an alternative scenario, involving the presence of a spiral and bar structure made of a mixture of stellar and gaseous components. This later scenario seems promising as it provides as well clues on the central engine feeding. Indeed, the bar within bar mechanism has been studied in details through N-body simulations of a stellar and gaseous component mixture (Athanasoula, 1994). As gas is pushed inward along the bar, it forms a bar-unstable disc on a smaller scale, which will generate in turn a smaller bar. This mechanism could repeat itself on scales which are smaller and smaller. The dynamical behavior of such a system has been modeled with various configurations (Combes, 1994b; Friedli, 1996), the prediction being that the innermost disc is in relation with the presence of a bar about twice as large (Combes, private communication). In the case of NGC 1068, we noticed that each of the radial brightness distributions in J and H (Fig. 1f) is quite well fitted by two exponential disks with characteristic radii of $r_e = 220$ pc, $r_i = 19$ pc. Considering that the J band is mainly a tracer of stars, then the scale-length of the inner exponential disk, 19 pc, is about what would be obtained after a few rotations of a 40 pc bar, the size of the elongated NS feature. Under this scenario, the $2.2 \mu\text{m}$ emission would be related as well to the stellar component, although the presence of both gas and dust taking part in the dynamics is not unlikely.

Detailed information on the kinematics of the innermost regions are required to distinguish between the two possibilities, calling for the obtainment of 2D-spectroscopic data sets at high angular resolution. Yet, the presence of two other bar/spiral systems on larger scales in NGC 1068 and the natural explanation for inward mass transfer, lead us to conclude that the S-shaped structure may represent the third level of an interwoven system of bars, spiral and ring structures, bringing material inward to build up and feed the black-hole/accretion-disk system (Schlos-

³ 600K is the temperature of grains at $4 \cdot 10^{-4}$ pc of a B2 star, a distance one thousand times smaller than the mean distance between

stars if the luminosity of $1.8 \cdot 10^{10} L_\odot$ was accounted for by a cluster of B2 stars within the $0''.2 \times 0''.3$

man et al. 1989). This constitutes the first direct suggestion of the existence of a micro-barréd/spiral structure in an AGN.

Acknowledgements. We are gratefully indebted to Z. Tsvetanov for making available to us the fully calibrated and aligned HST/WFPC2 images and to J.P. Véran for reconstructing PSFs with his powerful method. We warmly thank the CFHT team who allowed successful Pueo observations. Thanks are extended to the referee, J. Gallimore, who made several useful suggestions and to C. and G. Robichez for pertinent comments that helped improving the manuscript.

References

- Antonucci R., 1993, ARAA 31, 473
- Athanassoula E., 1994, in "Mass transfer Induced Activity in Galaxies", I. Shlosman Ed, Cambridge University Press, p. 143
- Blietz M., Cameron M., Drapatz S. et al., 1994, ApJ 421, 92
- Braatz J.A., Wilson A.S., Gezari D.Y., Varosi F., Beichman C.A., 1993, ApJ 409, L5
- Cameron M., Storey J.W.V., Rotaciuc V. et al., 1993, ApJ 419, 136
- Capetti A., Macchetto F.D. Axon D.J., Sparks W., Boksenberg A., 1995, ApJ 452, L87
- Capetti A., Macchetto F.D., Lattanzi M.G., 1997, ApJ 476, L67
- Chelli A., Perrier C., Cruz-Gonzales I., Carrasco L., 1987, A&A 177, 51
- Combes F., 1994a, in "The formation and Evolution of Galaxies", C. Muñoz & F. Sanchez Eds, Cambridge University Press, p. 317
- Combes F., 1994-b, in "Mass transfer Induced Activity in Galaxies", ed. I. Schlosman, Cambridge University Press, Cambridge, p. 170
- Dopita M.A., Sutherland R.S., 1995, ApJ 455, 468
- Efstathiou A., Rowan-Robinson M., 1994, MNRAS 212, 218
- Evans I.N., Ford H.C., Kinney A.L. et al., 1991, ApJ 369, L27.
- Friedli D., Martinet L., 1993, A&A 277, 27
- Friedli D., 1996, ASP Conf. Ser. 91, p 378
- Gallais P., 1991, PhD thesis, Université Paris 7
- Gallimore J.F., Baum S.A., O'Dea C.P., Pedlar A., 1996a, ApJ 458, 136
- Gallimore J.F., Baum, S.A., O'Dea C.P., Brinks E., Pedlar A., 1996-b, ApJ 462, 740
- Gallimore J.F., Baum, S.A., O'Dea C.P., 1997, Nat 388, 852
- Granato G.L., Danese L., Franceschini A., 1997, ApJ 486, 147
- Greenhill L.J., Gwinn C.R., 1997, Astrophy. Sp. Sc. 248, 261
- Heller C.H., Shlosman I., 1994, ApJ 424, 84
- Krolik J.H., Begelman M.C., 1986, ApJ 308, L55
- Lynds R., Faber S.M., Groth E.J. et al., 1991, ApJ 369, L31
- Macchetto F., Capetti A., Sparks W., Axon D.J., Boksenberg A., 1994, ApJ 435, L16
- Magain P., Courbin F., Sohy S., 1997, ESO Messenger 88, 28
- Marco O., Alloin D., Beuzit J.L., 1997, A&A 320, 399
- Mulchaey J.S., Wilson A.S., Bower G.A. et al., 1994, ApJ 433, 625
- Muxlow T.W., Pedlar A., Holloway A., Gallimore J., Antonucci R., 1996, MNRAS 278, 854
- Pier E.A., Krolik J.H., 1993, ApJ 418, 673
- Planesas P., Scoville N.Z., Myers S.T., 1991, ApJ 369, 364
- Nadeau D., Murphy D.C., Doyon R., Rowlands N., 1994, PASP 106, 909
- Rieke G.H., Lebofsky M.J., 1985, ApJ 288, 618
- Rigaut F., Arsenault R., Kerr J., et al., 1994, Proc. SPIE Vol. 2201, p. 149
- Roddiér F.J., Graves J.E., McKenna D., Northcott M.J., 1991, Proc. SPIE Vol. 1524, p. 248
- Rousset G., 1994, in Adaptive Optics for Astronomy, eds D. Alloin and J.M. Mariotti, Kluwer Acad. Pub., p. 115
- Shlosman I., Frank J., Begelman, M. C., 1989, Nat 338, 45
- Tacconi L.J., Genzel R., Blietz M. et al., 1994, ApJ 426, L77
- Thatte N., Quirrenbach A., Genzel R., Maiolino R., Tecza M., 1997, ApJ 490, 238
- Ulvestad J.S., Neff S.G., Wilson A.S., 1987, AJ 92, 22
- Lai O., Véran J.P., Rigaut F., Rouan D., et al., 1996, Proc. SPIE Vol. 2871, p. 859-870.,
- Véran J.P., Rigaut F., Maître H., Rouan D., 1997, Journ. of the Optic. Soc. of America A 14, 11
- Véran J.P., 1997, Thesis, Ecole Nationale Supérieure des Télécommunications and Paris 7
- Wilson A.S., Ulvestad J.S., 1987, ApJ 319, 105
- Young S., Packham C., Hough J.H., Efstathiou A., 1996, MNRAS 283, L1